Microwave Background Anisotropies from Scaling Seed Perturbations

Ruth Durrer and Mairi Sakellariadou

Département de Physique Théorique
Université de Genève
24 quai Ernest Ansermet, CH-1211 Genève 4, Switzerland

Abstract

We study microwave background anisotropies induced by scaling seed perturbations in a universe dominated by cold dark matter. Using a gauge invariant linear perturbation analysis, we solve the perturbation equations on superhorizon scales, for CMB anisotropies triggered by generic gravitational seeds. We find that perturbations induced by seeds — under very mild restrictions — are nearly isocurvature. Thus, compensation, which is mainly the consequence of physically sensible initial conditions, is very generic.

We then restrict our study to the case of scaling sources, motivated by global scalar fields. We parameterize the energy momentum tensor of the source by "seed functions" and calculate the Sachs-Wolfe and acoustic contributions to the CMB anisotropies. We discuss the dependence of the anisotropy spectrum on the parameters of the model considered. Even within the restricted class of models investigated in this work, we find a surprising variety of results for the position and height of the first acoustic peak as well as for the overall amplitude. In particular, for certain choices of parameters, the spectrum resembles very much the well known adiabatic inflationary spectrum, whereas for others, the position of the first acoustic peak is significantly shifted towards smaller angular scales.

PACS numbers: 98.80-k 98.80.Hw 98.80C

1 Introduction

The origin of the large scale structure in the universe, is clearly one of the most important open questions in cosmology. Within the framework of gravitational instability, there are two currently investigated families of models to explain the formation of the observed structure. Initial density perturbations can either be due to "freezing in" of quantum fluctuations of a scalar field during an inflationary period [1], or they may be seeded by topological defects, which can form naturally during

a symmetry breaking phase transition in the early universe [2]. Inflationary fluctuations are produced at a very early stage of the evolution of the universe, and are driven far beyond the Hubble radius by inflationary expansion. Subsequently, they are not altered anymore and evolve freely according to homogeneous linear perturbation equations until late times. These fluctuations are termed "passive" and "coherent" [3]. "Passive", since no new perturbations are created after inflation; "coherent" since randomness only enters the creation of perturbations during inflation, subsequently they evolve in a deterministic and coherent manner.

On the other hand, in models with topological defects or other types of seeds, fluctuations are generated continuously and evolve according to inhomogeneous linear perturbation equations. The seeds are any non–uniformly distributed form of energy, which contributes only a small fraction to the total energy density of the universe and which interacts with the cosmic fluid only gravitationally. We will be particularly interested in the case of global topological defects, playing the role of seeds. The energy momentum tensor of the seed is determined by the defect (seed) evolution which, in general, is a non-linear process. These perturbations are called "active" and "incoherent" [3]. "Active" since new fluid perturbations are induced continuously due to the presence of the seeds; "incoherent" since the randomness of the non-linear seed evolution which sources the perturbations can destroy the coherence of fluctuations in the cosmic fluid.

The cosmic microwave background (CMB) anisotropies provide a link between theoretical predictions and observational data, which may allow us to distinguish between inflationary models and defect scenarios, by purely linear analysis. On large angular scales, both families of models predict an approximately scale-invariant Harrison-Zel'dovich spectrum [4, 5]. Although, perturbations from defect models are non-Gaussian, this signature is probably rather weak, especially on large scales, where cosmic variance is substantial, and its observation might be quite difficult.

Acoustic peaks have been extensively studied in inflationary models, where observations of amplitude and position of the peaks can be used to determine cosmological parameters [6]. Some studies of simplified models where perturbations are seeded by topological defects, have already appeared in the literature[7, 8].

In this paper, we present a general investigation of acoustic peaks for models with active perturbations. We estimate the Sachs-Wolfe and acoustic contributions. Our "seed functions", which determine the energy momentum tensor of the source are motivated from 3d numerical simulations of π_3 defects, textures [9, 10], in a universe dominated by cold dark matter (CDM). We restrict ourselves to scalar perturbations.

In section 2, we study CMB anisotropies triggered by generic gravitational seeds. In particular, we present the equation for the coefficients C_ℓ and discuss the Sachs-Wolfe contribution, the acoustic peaks and Silk damping. We solve the perturbation equations for super-horizon scales. Studying the Bardeen potentials Ψ and Φ, which describe the scalar geometry perturbations, we find that compensation is automatically obtained, i.e., that perturbations are nearly isocurvature. In section 3, we restrict our investigation to the case of global scalar fields, for which we deduce the power spectra of the seed functions from numerical simulations and analytical scaling arguments. The results obtained there apply for general scaling sources. In section 4, we present some numerical examples and discuss how the characteristics of the acoustic peaks depend on the model. We summarize our conclusions in section 5.

Notation: The Friedmann metric is given by $a^2(-dt^2 + \gamma_{ij}dx^i dx^j)$, where a denotes the scale factor, t is conformal time and γ is the metric of a three space with constant curvature K. We shall consider a universe dominated by cold dark matter and discuss the case $K = 0$ exclusively. An over-dot stands for derivative with respect to conformal time t, while prime denotes the derivative with respect to $kt \equiv x$. Subscripts (or superscripts) $_r$ ($^{(r)}$) and $_c$ ($^{(c)}$) indicate the baryon-radiation

plasma and CDM, respectively.

2 CMB anisotropies from seeds

The coefficients C_ℓ represent the angular power spectrum of CMB anisotropies. They can be given in terms of the expansion of the angular correlation function

$$\langle \frac{\delta T}{T}(\mathbf{n}) \frac{\delta T}{T}(\mathbf{n}') \rangle \Big|_{(\mathbf{n}\cdot\mathbf{n}'=\cos\vartheta)} = \frac{1}{4\pi} \sum_\ell (2\ell+1) C_\ell P_\ell(\cos\vartheta) \ .$$

We want to investigate these coefficients in models where the fluctuations are induced by seeds. We restrict ourselves to scalar perturbations, but this analysis is easily extended to include vector and tensor contributions.

If we neglect Silk damping in a first step and integrate the photon geodesics in the perturbed metric, gauge invariant linear perturbation analysis leads to [11, 12]

$$\begin{aligned} \frac{\delta T}{T}(\mathbf{x},\mathbf{n}) &= \Big[-\frac{1}{4} D_g^{(r)}(\mathbf{x}) - V_j(\mathbf{x}) n^j - (\Psi-\Phi)(\mathbf{x}) \Big]_i^f \\ &\quad + \int_i^f (\dot\Psi - \dot\Phi)(\mathbf{x}', t') d\tau \ , \end{aligned} \tag{1}$$

where over-dot denotes derivative with respect to conformal time t. Φ and Ψ are the Bardeen potentials, quantities describing the perturbations in the geometry, $\mathbf{V}$ is the peculiar velocity of the baryon fluid with respect to the overall Friedmann expansion and $D_g^{(r)}$ specifies the intrinsic density fluctuation in the radiation fluid. There are several gauge invariant variables which describe density fluctuations; they all differ substantially on super-horizon scales but coincide inside the horizon. D_g corresponds to the density fluctuation in the so-called "flat slicing", where the perturbation of the 3-dimensional Riemann scalar vanishes. The initial time is the time of decoupling, t_{dec} of baryons and radiation, which occured at a redshift of $z_{dec} \sim 1100$.

The final time values in the square bracket of Eq. (1) give rise only to monopole contributions and the dipole due to our motion with respect to the CMB and are disregarded in the following. Taking the Fourier transform of Eq. (1), we then obtain

$$\begin{aligned} \frac{\delta T}{T}(\mathbf{k},\mathbf{n}) = e^{i(\mathbf{k}\cdot\mathbf{n})t_0} [&\frac{1}{4} D_g^{(r)}(\mathbf{k}, t_{dec}) + \mathbf{V}(\mathbf{k}, t_{dec}) \cdot \mathbf{n} + (\Psi-\Phi)(\mathbf{k}, t_{dec}) \\ &+ \int_{t_{dec}}^{t_0} (\dot\Psi - \dot\Phi)(\mathbf{k}, t) e^{-i(\mathbf{k}\cdot\mathbf{n})t} dt] \ . \end{aligned} \tag{2}$$

The first term in Eq. (2) describes the intrinsic inhomogeneities on the surface of the last scattering due to acoustic oscillations prior to decoupling. It also contains contributions to the geometrical perturbations [7]. The second term describes the relative motions of emitter and observer. This is the Doppler contribution to the CMB anisotropies. It appears on the same angular scale as the acoustic term and we denote the sum of the acoustic and Doppler contributions by "acoustic peaks". The last two terms are due to the inhomogeneities in the spacetime geometry; the first contribution determines the change in the photon energy due to the difference of the gravitational potential at the position of emitter and observer. Together with the part contained in $D_g^{(r)}$ they represent the "ordinary" Sachs-Wolfe effect. The second

term accounts for red-shifting or blue-shifting caused by the time dependence of the gravitational field along the path of the photon (Integrated Sachs-Wolfe (ISW) effect). The sum of the two terms is the full Sachs-Wolfe contribution (SW).

On angular scales $0.1^\circ \lesssim \theta \lesssim 2^\circ$, the main contribution to the CMB anisotropies comes from the acoustic peaks, while the SW effect is dominant on large angular scales. For topological defects, the gravitational contribution is mainly due to the ISW. The "ordinary" Sachs Wolfe term even has the wrong spectrum, a white noise spectrum instead of Harrison–Zel'dovich [10].

From Eq. (2) the C_ℓ's are found to be

$$C_\ell = \frac{2}{\pi} \int \frac{< |\Delta_\ell(\mathbf{k})|^2 \rangle}{(2\ell+1)^2} k^2 dk \ , \tag{3}$$

with

$$\begin{aligned} \frac{\Delta_\ell}{2\ell+1} &= j_\ell(kt_0) \left[\frac{1}{4} D_g^{(r)}(\mathbf{k}, t_{dec}) + (\Psi - \Phi)(\mathbf{k}, t_{dec}) \right] - j'_\ell(kt_0) \mathbf{V}_r(\mathbf{k}, t_{dec}) \\ &\quad + \int_{t_{dec}}^{t_0} (\dot{\Psi} - \dot{\Phi})(\mathbf{k}, t') j_\ell(k(t_0 - t')) dt' \\ &= \frac{1}{4} D_g^{(r)}(\mathbf{k}, t_{dec}) j_\ell(kt_0) - j'_\ell(kt_0) \mathbf{V}_r(\mathbf{k}, t_{dec}) \\ &\quad + k \int_{t_{dec}}^{t_0} (\Psi - \Phi)(\mathbf{k}, t') j'_\ell(k(t_0 - t')) dt' \ ; \end{aligned} \tag{4}$$

j_ℓ denotes the spherical Bessel function of order ℓ and j'_ℓ stands for its derivative with respect to the argument.

On scales smaller than about 0.1^o, the anisotropies are damped due to the finite thickness of the recombination shell, as well as by photon diffusion during recombination (Silk damping). Baryons and photons are very tightly coupled before recombination and oscillate as one component fluid. During the process of decoupling, photons slowly diffuse out of over-dense into under-dense regions. To fully account for this process, one has to solve the Boltzmann equation (see, e.g. [12]). A reasonable approximation can however be achieved by multiplying the Δ_ℓ with an exponential damping envelope $\mathcal{D}_\gamma(k)$ which is given in Ref. [13].

We now discuss the calculation of the C_ℓ's for perturbations with seeds. Since the background contribution of the energy momentum tensor of the seeds vanishes, its components $\Theta_{\mu\nu}$ are gauge invariant perturbation variables. They can be decomposed into scalar, vector and tensor contributions. Here we restrict ourselves to scalar perturbations. We express the scalar degrees of freedom of $\Theta_{\mu\nu}$ in terms of the gauge invariant perturbation variables f_ρ, f_p, f_v, f_π, which parameterize the energy density, pressure, scalar velocity potential and anisotropic stress potential of seeds, respectively (see [11, 12]).

$$\Theta_{00} = M^2 f_\rho \tag{5}$$

$$\Theta_{i0}^{(s)} = M^2 f_{v,i} \tag{6}$$

$$\Theta_{ij}^{(s)} = M^2 [\{ f_p - (1/3)\Delta f_\pi \} \gamma_{ij} + f_{\pi,ij}] \ , \tag{7}$$

where Δ denotes the Laplacian with respect to the metric γ of the three space and M is a typical "mass", energy scale, of the seeds. The superscript $^{(s)}$ indicates that only the scalar contribution to Θ_{i0} and Θ_{ij} is obtained in this way. Numerical simulations show that the vector and tensor perturbations make up about 20% of

the energy momentum tensor on super–horizon scales [10]. Since we assume that the seeds interact with other matter components only gravitationally, the seed functions satisfy the following covariant conservation equations [12]

$$\dot{f}_\rho - \Delta f_v + (\dot{a}/a)(f_\rho + 3f_p) = 0 \quad (8)$$

$$\dot{f}_v + 2(\dot{a}/a)f_v - f_p - (2/3)\Delta f_\pi = 0 \ . \quad (9)$$

We consider the matter content of the universe as a two-fluid system: the baryons+radiation plasma, which prior to recombination is tightly coupled, and cold dark matter (CDM). Before recombination, the evolution of the perturbation variables in a spatially flat background, $\Omega = 1$, is described by [14]

$$\dot{D}_g^{(r)} - 3(c_r^2 - w_r)\frac{\dot{a}}{a}D_g^{(r)} + kV_r(1+w_r) = 0 \quad (10)$$

$$\dot{D}_g^{(c)} + kV_c = 0 \quad (11)$$

$$\dot{V}_r + (1-3c_r^2)\frac{\dot{a}}{a}V_r - k(\Psi - 3c_r^2\Phi) - k\frac{c_r^2}{(1+w_r)}D_g^{(r)} = 0 \quad (12)$$

$$\dot{V}_c + \frac{\dot{a}}{a}V_c - k\Psi = 0 \ , \quad (13)$$

where subscripts $_r$, $_c$ (superscript $^{(r)}$, $^{(c)}$) denote the baryon-radiation plasma and CDM, respectively; D and V are density and velocity perturbations; $w = p_r/\rho_r$, $c_s^2 = \dot{p}_r/\dot{\rho}_r$ and $\rho = \rho_r + \rho_c$. The geometrical perturbations Ψ and Φ can be separated into a part coming from standard matter and radiation (subscript $_m$), and a part due to the seeds (subscript $_s$).

$$\Psi = \Psi_m + \Psi_s \quad (14)$$

$$\Phi = \Phi_m + \Phi_s \ , \quad (15)$$

where Ψ_s and Φ_s are determined by the energy momentum tensor of the seeds. We find [12]

$$\Phi_m = \frac{4\pi G a^2}{k^2}[\rho_r D_g^{(r)} + \rho_c D_g^{(c)} - 3\{\rho_r(1+w_r) + \rho_c\}\Phi + 3\frac{\dot{a}}{a}k^{-1}\{\rho_r(1+w_r)V_r + \rho_c V_c\}] \quad (16)$$

$$\Psi_m = -\Phi_m \quad (17)$$

$$\Phi_s = \epsilon k^{-2}[f_\rho + 3\frac{\dot{a}}{a}f_v] \quad (18)$$

$$\Psi_s = -\Phi_s - 2\epsilon f_\pi \ , \quad (19)$$

where $\epsilon \equiv 4\pi G M^2$. This parameter has to be small to validate cosmological perturbation theory. In other words, the mass M has to be significantly smaller than the Planck mass. For global scalar fields, it actually turns out that the typical amplitude of geometrical perturbations is of the order of ϵ, so that the COBE normalization requires $M \sim 10^{16}$GeV. In this work, we neglect the contribution of neutrino fluctuations. Anisotropic stresses in the matter components are explicitly set to zero, $\Pi_m \equiv 0$, which implies Eq. (17). The anisotropic stresses in the source, f_π, can therefore not be compensated.

To solve the above system of equations, we need to specify initial conditions. For a given scale k, we choose the initial time t_{in} early enough, such that the perturbations are super-horizon and the universe is radiation dominated at t_{in}. We set $x = kt$ and denote by a prime the derivative w.r.t x. The super-horizon limit is thus the limit $x \ll 1$. Choosing (x, k) as independent variables, the perturbation equations reduce in this limit to

$$\begin{aligned}
D_g^{(r)\prime} + \frac{4}{3} V_r &= 0 && (20)\\
D_g^{(c)\prime} + V_c &= 0 && (21)\\
V_r' + (\Phi - \Psi) - \frac{1}{4} D_g^{(r)} &= 0 && (22)\\
V_c' + V_c/x - \Psi &= 0 && (23)\\
\Psi_m + \Phi_m &= 0 && (24)\\
\Phi_s &= \epsilon k^{-2} (f_\rho + 3 f_v/t) && (25)\\
\Phi &= \frac{x^2}{6} \Phi_s + V_r/x && (26)\\
\Psi + \Phi &= 2\epsilon f_\pi \ . && (27)
\end{aligned}$$

If f_ρ, f_v and f_π are differentiable in the vicinity of $x = 0$, we can solve the above system exactly. We take the derivative of Eq. (20) and replace V_r' with Eq. (22). Using Eqs. (26, 27, 25) we then find

$$D_g^{(r)\prime\prime} + \frac{2}{x} D_g^{(r)\prime} = \epsilon (2 f_\pi + \frac{x^2}{3k^2} f_\rho + \frac{x}{k} f_v) \ . \qquad (28)$$

Differentiability now guarantees that the source term on the right hand side of Eq. (28) is given by $\epsilon A(k) x^\alpha$ + higher orders. We then obtain to lowest order in x

$$\begin{aligned}
D_g^{(r)} &= \frac{\epsilon A(k)}{(\alpha+2)(\alpha+3)} x^{\alpha+2} && (29)\\
V_r &= -\frac{3\epsilon A(k)}{4(\alpha+3)} x^{\alpha+1} && (30)\\
\Phi - \Psi &= \frac{3\epsilon A(k)(\alpha+1)}{4(\alpha+3)} x^\alpha \ . && (31)
\end{aligned}$$

On the other hand, the seed perturbations are of the order of

$$\Phi_s \ , \ \Psi_s \propto \epsilon A(k) x^{\alpha-2} \gg \Phi \ , \ \Psi \ , \qquad (32)$$

if $f_\pi \lesssim (x^2/3k^2) f_\rho + (x/k) f_v$. For scaling sources, we shall see that these two terms are of the same order of magnitude. In other words, $\Phi \ll \Phi_s$ and, if f_π is not extremely large, $\Psi \ll \Psi_s$ on super-horizon scales. The main reason for this finding certainly lies in choosing the correct initial conditions which have to vanish in the absence of sources. We could always add a homogeneous contribution to $D_g^{(r)}$ which would destroy this behaviour. We consider this choice of initial conditions as the most natural way to obtain compensation: the presence of matter and radiation reduces the Bardeen potentials on super-horizon scales by a factor x^2. Only the contribution $\Phi + \Psi = -2\epsilon f_\pi$, which is due to anisotropic stresses, cannot be compensated by matter and radiation. If $f_\pi \neq 0$, there is compensation provided $f_\pi \leq \max(f_\rho t^2 \ , \ f_v t)$.

We therefore conclude that seeds, which are uncorrelated on super-horizon scales, are compensated by the presence of matter and radiation, where we define compensation as the suppression of the total Bardeen potentials by a factor x^2 with respect to Φ_s, Ψ_s. In this sense, the type of seed perturbations discussed here are nearly isocurvature fluctuations.

Within the context of scaling sources (seed functions with white noise spectra), the basic ingredient which leads to compensation, is not the absence of perturbations on very large scales or on very early times, but the fact that we only consider the particular solution of the second order differential equation for the perturbation variable $D_g^{(r)}$. Clearly, a homogeneous contribution to $D_g^{(r)}$ can destroy this finding. In our case, perturbations are induced by the presence of the seeds, and therefore these initial conditions are the most physical ones.

This result is important, since compensation has usually been understood either as a consequence of the integral constraint [15, 16, 3] or as a consequence of causality of the source perturbations[17]. In our work compensation arises naturally for scaling sources and it can be generalized to sources with arbitrary spectra which satisfy

$$f_\pi \leq \max(f_\rho t^2 \ , \ f_v t) \ . \tag{33}$$

Clearly for $\Pi = 0$, which is the most natural assumption for non-relativistic cosmic fluids, f_π has to be small since it cannot be compensated, $\Phi, \Psi \gtrsim \mathcal{O}(\epsilon f_\pi)$. If f_π is larger than the limit given in Eq. (33), then $\Pi \neq 0$ is a necessary but not sufficient condition for compensation to occur. We know of one example, namely relativistic collisionless particles, where compensation can take place for certain choices of f_π, due to the presence of anisotropic stresses Π (see appendix). Collisionless particles are special in that they interact with each other and with the seeds only through gravity. In general, if particle interactions other than gravity determine Π, we do not expect compensation, since by definition the seeds interact with the cosmic fluid only through gravity.

3 CMB anisotropies induced by scaling sources

We now restrict our study to scaling seeds. We first discuss as motivating example global scalar fields which, depending on their number of degrees of freedom, can lead to global topological defects during a symmetry breaking phase transition in the early universe [2]. We shall, however, only make use of the general behaviour of the seed functions $f_\bullet$ which we call "scaling". In the absence of any intrinsic length scale other than the cosmic horizon, this is the behaviour which the seed functions assume by dimensional reasons.

We consider an N-component scalar field with potential $V = \lambda(\phi^2 - \eta^2)^2$. In the σ-model approximation, the equation of motion for ϕ can be expressed solely in the dimensionless variable $\beta = \phi/\eta$ [10]. In terms of β the energy momentum tensor of the scalar field is given by

$$\Theta_{\mu\nu} = \eta^2 \left(\beta_{,\mu}\beta_{,\nu} - \frac{1}{2} g_{\mu\nu} \beta^{,\lambda}_{,\lambda} \right) \ . \tag{34}$$

Defining $M^2 \equiv \eta^2$, the functions $f_\bullet$ result in

$$f_\rho(\mathbf{k}) \ = \ \frac{1}{2}\mathcal{F}\left[\dot{\beta}^2 + (\nabla\beta)^2)\right]$$

$$
\begin{aligned}
f_p(\mathbf{k}) &= \frac{1}{2}\mathcal{F}\left[\dot{\beta}^2 - \frac{1}{3}(\nabla\beta)^2)\right] \\
f_v(\mathbf{k}) &= -\frac{i}{k^2}k^j\mathcal{F}\left[\dot{\beta}\beta_{,j}\right] \\
f_\pi(\mathbf{k}) &= -\frac{3}{2k^4}k_ik_j\mathcal{F}\left[\beta_{,i}\,\beta_{,j} - \frac{1}{3}\delta_{ij}(\nabla\beta)^2\right] \ , \qquad (35)
\end{aligned}
$$

where $\mathcal{F}[g]$ denotes the Fourier transform of g, defined by $g(k) = V^{-1/2}\int e^{ikx}g(x)d^3x$. In what follows, the Fourier transform of the seed functions $\mathcal{F}[f_\bullet]$, will be denoted simply by $f_\bullet$.

On super-horizon scales β and $\dot{\beta}$ are assigned random initial values, so they have white noise spectra initially. $\nabla\beta$ clearly has a k^2-spectrum. However, using the convolution theorem one finds that $(\nabla\beta)^2$ has a white noise spectrum. Therefore, both f_ρ and f_p have white noise spectra on super-horizon scales. From the above expressions for f_v we find

$$
f_v = \frac{(2\pi)^3k^j}{\sqrt{V}k^2}\int d^3q\dot{\beta}(\mathbf{q})\beta(\mathbf{q}-\mathbf{k})(q-k)_j \ .
$$

Expanding this expression in lowest order in k using that β and $\dot{\beta}$ have white noise spectra, we find that the term of order k^0 in the integral vanishes and the lowest order contribution to the integral is linear in k_j, so that f_v also has a white noise spectrum on super-horizon scales. By similar arguments one can deduce that f_π has a white noise spectrum on super-horizon scales.

The dimensions of f_ρ and f_p in physical space are $(\text{length})^{-2}$, therefore in k-space, f_ρ and f_p have dimensions $(\text{length})^{-1/2}$. Since on super-horizon scales ($kt \ll 1$), these functions have white noise spectra, they must behave as $1/\sqrt{t}$. The corresponding arguments lead to a super-horizon behaviour for $f_v \propto \sqrt{t}$ and $f_\pi \propto t^{3/2}$. So the power spectra of the seed functions behave like

$$
\begin{aligned}
\langle|f_\rho|^2\rangle &= A_1^2\ t^{-1}\ F_1(x) \\
\langle|f_p|^2\rangle &= A_2^2\ t^{-1}\ F_2(x) \\
\langle|f_v|^2\rangle &= A_3^2\ t\ F_3(x) \\
\langle|f_\pi|^2\rangle &= A_4^2\ t^3\ F_4(x) \ , \qquad (36)
\end{aligned}
$$

where we choose the dimensionless constants A_i to be positive and such that $F_i(0) = 1$. The power spectra of the functions $f_\bullet$ do not depend on the direction of $\mathbf{k}$, thus the F_i's are even functions of $x = kt$. Furthermore, since the energy momentum tensor of the source decays inside the horizon, we know that $F_i \to 0$ for $x \to \infty$. This behaviour of f_ρ, f_p and f_v has also been found by numerical simulations.

The temporal behaviour of f_ρ and f_p can also be understood from the following argument: the $k = 0$ component of f_ρ just corresponds to the average energy density multiplied by $\sqrt{V}$ and is thus proportional to $V^{1/2}/t^2$. On super-horizon scales, $f_\rho(k)$ is white noise superimposed on this average. The number N of independent patches in V is V/t^3 and hence the amplitude of $f_\rho(k)$ is proportional to $V^{-1/2}/(t^2N^{-1/2}) \propto t^{-1/2}$. The same arguments hold for f_p. From numerical simulations [10] for π_3 defects, global textures, one finds that the average of $\dot{\beta}^2$ over a shell of radius k can be modeled on super-horizon scales by

$$
\langle|\dot{\beta}^2|^2\rangle(k,t) \sim \frac{2}{t}. \qquad (37)
$$

We define a seed to be scaling if the power spectra of the seed functions behave as in Eq. (36). We expect this scaling behaviour to be valid not only for global scalar fields, but also for (local) cosmic strings. However, since the only decay mechanism for cosmic strings is through emission of gravitational radiation, we expect the functions F_i to decay slower on sub-horizon scales, than in the case of global fields, which decay very efficiently into Goldstone bosons.

The system given by Eq. (20) to (27) can be solved analytically if the stochastic variables $f_\bullet$ are replaced by the square root of their power spectra. The results are thus to be taken with a grain of salt. But we believe that the r.h.s. of the following equations are good approximations to the square roots of the power spectra of the corresponding stochastic variables on the l.h.s., since, as we argue below, this coherence assumption does not significantly influence the results on super–horizon scales. Inserting the square roots of Eqs. (36) in the system (20) to (27), one finds in the limit $x \ll 1$

$$\begin{aligned}
\Phi_s &= \epsilon(A_1 + 3A_3)k^{-3/2}x^{-1/2} && (38)\\
\Psi_s &= -\epsilon(A_1 + 3A_3 + 2A_4x^2)k^{-3/2}x^{-1/2} && (39)\\
D_g^{(r)} &= \frac{16}{189}\epsilon(2A_4 + \frac{1}{3}A_1 + A_3)k^{-3/2}x^{7/2} && (40)\\
D_g^{(c)} &= \frac{2}{63}\epsilon(4A_4 + \frac{5}{21}A_1 + \frac{5}{7}A_3)k^{-3/2}x^{7/2} && (41)\\
V_r &= -\frac{2}{9}\epsilon(\frac{1}{3}A_1 + A_3 + 2A_4)k^{-3/2}x^{5/2} && (42)\\
V_c &= -\frac{\epsilon}{63}(28A_4 + \frac{5}{3}A_1 + 5A_3)k^{-3/2}x^{5/2} && (43)\\
\Phi &= \frac{1}{6}x^2\Phi_s + \frac{V_r}{x} && (44)\\
\Psi &= -\Phi - 2\epsilon A_4 k^{-3/2}x^{3/2}\ . && (45)
\end{aligned}$$

We use these results as initial conditions for the system (10) to (19). Eqs. (40) and (41) show, that the perturbations are in general non-adiabatic.

Due to the conservation equations (8) and (9), the constants A_i are not independent. Taking the sum of the ensemble averages of the conservation equation Eq. (8) multiplied by $f_\rho^\star$ (the complex conjugate of f_ρ), and its complex conjugate, we obtain

$$\begin{aligned}
&\frac{d}{dt}\langle|f_\rho|^2\rangle + k^2\langle f_\rho^\star f_v + f_\rho f_v^\star\rangle + 2\frac{\dot a}{a}\langle|f_\rho|^2\rangle \\
&\qquad +3\frac{\dot a}{a}\langle f_\rho^\star f_p + f_\rho f_p^\star\rangle \;=\; 0. \qquad (46)
\end{aligned}$$

Let us discuss the above equation on super-horizon scales where we can neglect the second term. Since $(d/dt)\langle|f_\rho|^2\rangle = -\langle|f_\rho|^2\rangle/t$, we find that the real part of $\langle f_\rho^\star f_p\rangle$ is negative. Furthermore, Schwarz inequality leads to

$$|A_2| \geq \frac{1}{6}|A_1| \ \text{ in the radiation era, and } |A_2| \geq \frac{1}{4}|A_1| \ \text{ in the matter era.} \quad (47)$$

Similarly, from Eq. (9) we conclude that the real part of $\langle f_v^\star f_p\rangle$ is positive and

$$|A_2| \geq \frac{5}{2}|A_3| \ \text{ in the radiation era, and } |A_2| \geq \frac{9}{2}|A_3| \ \text{ in the matter era.} \quad (48)$$

The equality sign is valid, if and only if

$$\langle f_\rho^\star f_p + f_\rho f_p^\star \rangle = -2\sqrt{\langle |f_\rho|^2 \rangle \langle |f_p|^2 \rangle} \ .$$

We call this condition, which requires that f_ρ and f_p are in perfect phase correlation "perfect coherence" between f_ρ and f_p. On super-horizon scales the spectrum of $k^2 f_v$ is much smaller than the spectrum of f_ρ/t; and thus $k^2 f_v \langle\langle f_\rho/t$, almost everywhere in the space of realizations. Hence, on super–horizon scales energy conservation (Eq. 8) yields

$$f_\rho(t) = \frac{a(t_{in})}{a(t)} f_\rho(t_{in}) - \frac{3}{a(t)} \int_{t_{in}}^{t} \dot{a}(t') f_p(t') dt' \ .$$

The question of coherence between f_ρ and f_p is thus reduced to the question of unequal time coherence of f_p and f_ρ themselves. Similarly, the coherence between f_v and f_p reduces to the unequal time coherence of each of these functions. We believe that for scaling sources, unequal time coherence is reasonably well maintained on super-horizon scales and therefore the equal signs in Eqs. (47) and (48) are probably valid on sufficiently large scales. Numerical simulations for global scalar fields and the large N limit (see [18]) support this hypothesis.

We now address the effect of unequal time coherence, $\langle f_i(t) f_j(t') \rangle$, on the resulting power spectrum C_ℓ. To simplify the relevant equations, we neglect here the short matter dominated period before decoupling and we also neglect baryons, such that $c_r^2 = w_r = 1/3$. The dynamical components during the tight coupling epoch are thus reduced to radiation and seeds. A WKB solution of the evolution equations then gives

$$\begin{aligned} D_g^{(r)}(k,x) &= \frac{4}{\sqrt{3}} \int_0^x dx' [\Phi(x') - \Psi(x')] \ sin((x-x')/\sqrt{3}) \\ V_r(k,x) &= -\int_0^x dx' [\Phi(x') - \Psi(x')] \ cos((x-x')/\sqrt{3}) \ , \end{aligned} \tag{49}$$

where we set $\Phi(0) = \Psi(0) = D_g^{(r)} = 0$.
This actually just reformulates our simplified system of equations in terms of two integral equations, since the Bardeen potentials Φ and Ψ are given in terms of $D_g^{(r)}$, V_r and the source functions as follows

$$\begin{aligned} \Phi - \Psi &= \frac{2}{6+x^2}\left(\frac{3}{2} D_g^{(r)} + \frac{6}{x} V_r\right) + 2\epsilon\left(\frac{x^2}{k^2(6+x^2)} f_\rho + \frac{3x}{k(6+x^2)} f_v + f_\pi\right) \\ &= \frac{2}{6+x^2}\left(\frac{3}{2} D_g^{(r)} + \frac{6}{x} V_r\right) + \frac{2x^2}{6+x^2} \Phi_s + 2\epsilon f_\pi \ . \end{aligned} \tag{50}$$

As we have seen earlier, it is a very bad approximation to replace Φ and Ψ by the corresponding source potentials Φ_s and Ψ_s, since this does not take care of the compensation.

Applying the Hu and Sugiyama formalism [6] for topological defects [3], we obtain within our approximation ($\Omega_b = 0$, purely radiation dominated)

$$\begin{aligned} \frac{\Delta_\ell(k)}{2\ell+1} &= \int_0^{x_{dec}} dx [\Phi(x) - \Psi(x)] \{ \frac{j_\ell(x_0 - x_{dec})}{\sqrt{3}} \sin(\frac{x_{dec} - x}{\sqrt{3}}) \\ &\quad - j_\ell'(x_0 - x_{dec}) \cos(\frac{x_{dec} - x}{\sqrt{3}}) \} \end{aligned}$$

$$+[\Psi(x_{dec})-\Phi(x_{dec})]j_\ell(x_0-x_{dec})$$
$$+\int_{x_{dec}}^{x_0} dx[\Psi'(x)-\Phi'(x)]\; j_\ell(x_0-x), \qquad (51)$$

where $x_{dec}=kt_{dec}$, $x_0=kt_0$. The times t_{dec} and t_0 denote the time of decoupling and today respectively. The somewhat more involved formula which takes into account the presence of baryons and CDM, can be found in [3].

Assuming coherence, the power spectrum C_ℓ can be calculated by squaring $\Delta_\ell/(2\ell+1)$ obtained from Eq. (51), where each variable is replaced by the square root of its power spectrum. On the other hand, for totally incoherent perturbations, one should instead use [3]

$$\begin{aligned} C_\ell &= \int dk k^3 \int_0^{x_{dec}} dx P_r(\Phi-\Psi)\{\frac{j_\ell(x_0-x_{dec})}{\sqrt{3}}\sin(\frac{x_{dec}-x}{\sqrt{3}}) \\ &\quad -j'_\ell(x_0-x_{dec})\cos(\frac{x_{dec}-x}{\sqrt{3}})\}^2 \\ &\quad +\int dk k^2[P(\Psi-\Phi)(t_{dec})]\; j_\ell^2(x_0-x_{dec}) \\ &\quad +\int dk k^3[j'_\ell(x_0-x_{dec})j_\ell(x_0-x_{dec})[P_r(\Psi-\Phi)](x_{dec})] \\ &\quad +\int dk \int_{x_{dec}}^{t_0} dx k^2 P_r(\Psi'-\Phi')j_\ell^2(x_0-x)\;, \end{aligned} \qquad (52)$$

where $P(X)\equiv\langle|X|^2\rangle(k,t)$ denotes the power spectrum of the variable X and $P_r(X)$ is the power spectrum of X integrated over a short time period Δt (see [3]).

We now want to illustrate the difference of the two approaches in our simplified pure radiation model. For pure radiation we can derive the following second order equation for $D_g^{(r)}$:

$$\begin{aligned} D_g^{(r)''}+\frac{12}{(6+x^2)x}D_g^{(r)'}-\frac{2-x^2/3}{6+x^2}D_g^{(r)} &= \frac{8\epsilon}{3}\left[\frac{x^2}{k^2(6+x^2)}f_\rho+\frac{3x}{k(6+x^2)}f_v+f_\pi\right] \\ &= \frac{8}{3}(\epsilon f_\pi+\frac{x^2}{6+x^2}\Phi_s)\;, \end{aligned} \qquad (53)$$

with general solution

$$D_g^{(r)}=\frac{8}{3}\epsilon\int_0^x f(x')G(x,x')dx'\;, \qquad (54)$$

where $f(x)\equiv f_\pi(x)+(x^2/6\epsilon)\Phi_s/$ and $G(x,x')$ denotes the Green's function

$$G(x,x')=\frac{\sqrt{3}x'}{(6+x'^2)x}\left[(12+xx')\sin\left(\frac{x-x'}{\sqrt{3}}\right)+2\sqrt{3}(x+x')\cos\left(\frac{x-x'}{\sqrt{3}}\right)\right]\;. \qquad (55)$$

The power spectrum of $D_g^{(r)}$ is therefore

$$\langle|D_g^{(r)}|^2\rangle=\frac{64}{9}\epsilon^2\int_0^x\int_0^x dx'dx''\langle f(x')f^\star(x'')\rangle G(x,x')G(x,x'')\;. \qquad (56)$$

Assuming total coherence, Eq. (56) takes the form

$$\langle|D_g^{(r)}|^2\rangle = [\frac{8}{3}\epsilon\int_0^x dx'\sqrt{\langle|f(x')|^2\rangle}G(x,x')]^2\;. \qquad (57)$$

On the other hand, assuming complete decoherence,

$$\langle f(x) f^{\star}(x') \rangle = \delta(x - x') \int_{x}^{x+\Delta x} dx \langle |f(x)|^2 \rangle \ , \tag{58}$$

leads to the power spectrum

$$\langle |D_g^{(r)}|^2 \rangle = \frac{64}{9} \epsilon^2 r \int_0^x dx' \langle |f(x')|^2 \rangle G^2(x, x') \ , \tag{59}$$

where we have chosen $\Delta x = rx$. We further assume also complete decoherence between different source functions,

$$\langle f_\pi f_v \rangle = \langle f_\pi f_\rho \rangle = \langle f_v f_\rho \rangle = 0 \ . \tag{60}$$

In Figs. 1a and 1b we plot $|D_g^{(r)}|^2 k^3$ versus kt_{dec} under the assumption of total coherence and complete decoherence respectively. The role of the coherence assumption on the characteristics of the power spectrum is shown in Fig. 2. Clearly, complete decoherence shifts the first acoustic peak to smaller angular scales, and reduces substantially its height. Furthermore, secondary peaks are completely washed out.

A realistic defect model will always lay somewhere between these two extremes. We suppose however, motivated by numerical simulations of textures and the large N limit, that the texture example is closer to the completely coherent case. In the next section we thus restrict ourselves to perfect coherence.

4 Numerical examples

In this section we study how the characteristics of the acoustic peaks depend on the values of the dimensionless constants A_i and the form of the functions F_i, which determine the power spectra of the seed functions (see Eq. (36)). A crucial question is whether there is a set of parameters for which the position and amplitude of the primary acoustic peak are similar to those predicted by an adiabatic inflationary model.

As we discussed earlier, the functions F_i are normalized such that $F_i(0) = 1$, and $F_i \to 0$ for $x \to \infty$. Numerical simulations for global textures [10] suggest that in the case of global scalar fields, the functions F_i have power law decay. However, for generic scaling sources, one could also consider the case of exponential decay. As we shall show, the form of these functions affects the features of the power spectrum significantly. In general, we find that if F_i have an exponential decay, the position of the primary peak is within the range predicted by adiabatic inflationary models, at $\ell \sim 220$. On the other hand, if F_i have a power law decay, as it seems to be for global topological defects, the position of the first acoustic peak is clearly shifted to smaller angular scales, at around $\ell \sim 300$ to 400. The amplitude of fluctuations decreases by up to a factor of 500 if we choose an exponential decay law for the seed functions. This is due to the fact that in this case the decay is very fast and erases almost all substantial seed contribution. The sensitivity of the overall amplitude of CMB perturbations on the parameters is extremely important especially if one wants to rule out defect models with biasing arguments!

In figures 3 to 8, we show the resulting power spectra for different set of dimensionless constants A_i, with the seed functions having either exponential or power law decay. The dashed line indicates the SW contribution, the dashed-dotted line is the contribution from the acoustic peaks, and their sum is drawn as solid line.

In Fig. 3a we choose an exponential decay for all the seed functions, $F_i(x) = \exp(-x^2)$, and a set of constants $A_1 = 3, A_3 = -0.6, A_4 = 0$. The position of the primary peak is at $\ell \sim 200$, while the relevant height of the first peak with respect to the SW plateau is ~ 25. Using the same set of constants A_i, however choosing a power law decay for the seed functions, $F_i(x) = [1. + (1./(2\pi)^2)x^2]^{-1}$, we see in Fig. 3b that the peak is displaced to smaller angular scales, at ~ 330, while the relative amplitude of the acoustic peak with respect to the SW plateau remains ~ 25. Also the features of the secondary peaks are different. While in Fig. 3a the second and third peaks have almost the same height, in Fig. 3b the second peak has almost completely disappeared. In both cases, the spectral index of the plateau, in the range $\ell \sim 2 - 20$ is $n \sim 1$, consistent with observations.

Now, selecting a slightly different set of dimensionless constants, we see that the predicted power spectrum is very different. In Fig. 4 we show the power spectrum for $A_1 = 3, A_3 = -0.7, A_4 = 0$, and the same power law decay for the functions F_i as in Fig. 3b. The primary peak is again at rather large angular scales, ~ 350, but the height of the peak is different, and the spectral index clearly deviates from 1.

A very interesting case is displayed in Fig. 5a, where we see that both the position and the amplitude of the first acoustic peak, agreed with those predicted by a generic inflationary model. Here, $A_1 = 3, A_3 = 1, A_4 = 2$, and $F_i(x) = \exp(-x^2)$. The primary peak is at $\ell \sim 200$ and its relative amplitude is at ~ 4. The second peak is almost completely washed out and the spectral index in the range $\ell \sim 2 - 20$ is very close to 1. This power spectrum, where perturbations are generated by scaling seeds, is quite similar to one resulting from an adiabatic inflationary model. Considering the same set of parameters and a somewhat slower exponential decay for the functions F_i given by $F_i(x) = exp(-0.5x^2)$, we find (Fig. 5b) that both, the position and relative amplitude of the first peak with respect to the SW plateau, remain the same as in Fig. 5a, whereas the Sachs Wolfe plateau is somewhat prolonged. This simple example shows that it may well be possible to "manufacture" inflationary spectra by a suitable choice of seed functions. A point which has already been realized in Ref. [19]. It is thus extremely important to further constrain the seed functions of defect models by numerical simulations and/or the large N limit. It may well be that the requirement of power law decay of the seed functions, excludes the inflationary position of the first acoustic peak. With the same parameters A_i and a power law decay $F_i(x) = [1 + (1/(2\pi)^2)x^2]^{-1}$, the primary peak is at $\ell \sim 320$, while the relative height of the peak is about 8, Fig. 5c.

We have also considered the values for the parameters A_i which are suggested by the conservation equations and perfect coherence, choosing a power law decay, $F_i(x) = [1 + (1/(2\pi)^2)x^2]^{-1}$. We find that the sign of A_3 does not affect the features of the power spectrum. In Fig. 6a $A_1 = 3, A_3 = -1/6, A_4 = 1/(2(2\pi)^2)$, while in Fig. 6b $A_1 = 3, A_3 = 1/6, A_4 = 1/(2(2\pi)^2)$. In both these cases, the peak is at $\ell \sim 300$, and its amplitude is ~ 8.

Finally, to illustrate the variety of results which can be obtained by parameter variation within a simple family of seed functions, we show a rather extreme case in Fig. 7, where $A_1 = 3, A_3 = -1., A_4 = 0$ and $F_i(x) = exp(-x^2)$. Here we see no acoustic peaks at all. However, this is a rather particular case, since with this choice of parameters, all the variables $\Phi_s, \Psi_s, D_g^{(r)}, D_g^{(c)}, V_r$ and V_c vanish initially (see Eqs. (38) to (45)).

To analyze the dependence of the characteristics of the power spectrum on the seed functions in a somewhat more systematic way, we have calculated the C_ℓ's for a grid of values $-A_1 \leq A_3, A_4 \leq A_1$ with spacing $0.2A_1$ and fixed functions $F_i = 1/(1+(x/(2\pi))^2)$. We fitted the resulting C_ℓ for $2 \leq \ell \leq 20$ to the simple power law behaviour arising in inflationary models, $C_\ell \propto \Gamma(\ell + (n-1)/2)/\Gamma(\ell + (5-n)/2)$. We find that for $|A_4| \geq 0.4A_1$, the χ^2 of the fit is unacceptably high: $\chi^2 \sim 3$ to 4 for

$|A_4| = 0.4A_1$, and more than 10 for even larger anisotropic stresses. We allow for a relative error of 0.05. However, χ^2 depends only weakly on the value of A_3 (see Fig. 8). We therefore restrict the parameter range for A_4 to $-0.3A_1 \leq A_4 \leq 0.3A_1$. The spectral index is in good agreement with observations, $1 \leq n \leq 1.4$ (see Figs. 9a and 9b).

We find positions of the first acoustic peak in the range $260 \leq \ell_{peak} \leq 520$. For the choice of seed functions with power law decay on sub-horizon scales (which is also indicated from numerical simulations and from the large N limit), we never obtain the peak at the adiabatic inflationary position of ~ 220, and values $l_{peak} < 300$ are only found for very small A_4 (see Fig. 10).

We define the quantity $\ell_{peak}(\ell_{peak}+1)C_{\ell_{peak}}/(110C_{10})$ as a measure for the height of the acoustic peak. This quantity is very model dependent and assumes, within the small class of models investigated in our parameter study, all values between 0.1 (for $A_4 = 0$ and $A_3 = A_1$, i.e., virtually no discernible peak) and 11 (see Figs. 11a and 11b). For fixed A_3, the peak height is a steeply raising function of $|A_4|$. Only values $|A_4| < 0.1A_1$ lead to peak heights below 6.

It is interesting to note, that also the absolute amplitude of the spectrum is sensitively depending on the ratios A_4/A_1 and A_3/A_1. For $A_4 = 0$ the amplitude $110C_{10}$ varies from $0.002\epsilon^2 A_1^2$ for $A_3 = -0.2A_1$ to $0.8\epsilon^2 A_1^2$ for $A_3 = A_1$. If $A_4 \neq 0$, the amplitude does not depend very strongly on A_3 and grows from $\sim 0.4\epsilon^2 A_1^2$ for $|A_4| = 0.1A_1$ to $\sim 4\epsilon^2 A_1^2$ for $|A_4| = 0.3A_1$ (see fig. 12). This finding is important for the biasing problem of structure formation. Sometimes, defect models have been claimed to be ruled out, since they would not lead to large enough matter density fluctuations, if normalized to the COBE experiment on very large scales. This normalization fixes the only free parameter of a given model, namely the symmetry breaking scale and therefore ϵ. In our work, we have seen that the Sachs Wolfe fluctuations in the CMB are largely governed by A_4, the amplitude of anisotropic stresses. The density fluctuations in the dark matter, however, are induced by $\dot{\phi}^2$ alone (see, e.g. [11]), which is determined entirely by A_1 and A_2. Defect models, with somewhat small anisotropic stresses, e.g., $A_4 < 0.05A_1$, which are actually quite natural, but difficult to resolve numerically, may explain the different bias factors obtained from numerical simulations in [20, 10].

5 Conclusions

In this paper we analyzed with some generality the CMB anisotropies induced in models with scaling sources for an $\Omega = 1$, cold dark matter cosmological model.

Within the framework of gauge invariant perturbation theory it turns out that compensation is a consequence of "natural" initial conditions. By "natural" we mean that we only consider that part of the solution induced by the source itself and do not add an arbitrary homogeneous contribution. In this case, we have found that the total Bardeen potentials are reduced by a factor $x^2 = (kt)^2$ with respect to the potentials generated by the source alone. One may think at first sight that such a result is unphysical, acausal, however it just reflects that also the initial condition of a perfect Friedmann universe is acausal.

Even restricting ourselves to the case of scaling sources, we found that the resulting power spectrum depends significantly on the model parameters. In particular, if the seed functions decay exponentially, the position of the first acoustic peak is at $\ell \sim 220$ as in inflationary models. Adjusting the amplitude of the seed functions,

we can also obtain a peak height consistent with inflationary perturbations.

On the other hand, if the seed functions have a power law decay, as numerical simulations of global textures [10] as well as the large N limit [18] indicate, the position of the first peak is within the range $260 \leq \ell_{peak} \leq 500$. Its amplitude depends sensitively on the parameters of the seed functions which, for a specific model, have to be determined by involved numerical simulations. In our analysis we encountered amplitudes in the range $0.1 \leq \ell_{peak}(\ell_{peak}+1)C_\ell^{peak}/(110C_{10}) \leq 25$.

We also found that the total amplitude of CMB anisotropies produced depends strongly on the amplitude of anisotropic stresses of the seed. Whereas, the source term leading to CDM density fluctuations is given by $f_\rho + 3f_p$, i.e, determined by $A_1 + 3A_2$ on large scales. Therefore, the relation between the COBE normalization of the model and the bias factor depends sensitively on the ratio $A_4/(A_1+3A_2)$, which may depend on details of the model.

These results are obtained under the assumption of perfect coherence. This hypothesis seems reasonable for global scalar fields as also the large N limit indicates [18]. On the other hand, assuming complete decoherence, the position of the first peak is shifted to smaller angular scales, its amplitude is reduced and secondary peaks are washed out. A realistic situation may lay somewhere between the two extremes.

The examples with power law seed functions which we discussed in this paper were motivated by numerical simulations of global textures with vacuum manifold $\mathbf{S}^3$. Apart from the scaling behaviour on very large and very small scales, which should be the same for all global defects, we do not know to what extend the seed functions depend on this particular choice.

Acknowledgment It is a pleasure to thank Alejandro Gangui and Martin Kunz for helpful suggestions. We also thank Nathalie Deruelle, Maurizio Gasperini and Gabriele Veneziano for stimulating discussions. This work is partially supported by the Swiss NSF. M.S. acknowledges financial support from the Tomalla foundation.

APPENDIX

A Compensation for relativistic collisionless particles

In this appendix we show how compensation arises in the case of relativistic collisionless particles.

We consider a universe dominated by massless (*i.e.* relativistic) collisionless particles, with scalar perturbations induced by seeds. We assume seeds consisting of massless particles conformally coupled to gravity. In this case, the time dependence of the seed functions is given by $f_\bullet \propto 1/a^2 \propto 1/t^2$ (t denotes conformal time).

The evolution of perturbations is determined by the collisionless Bolztmann equation, which reads [12]

$$\partial_t \mathcal{M}(\mu,k,t) + ik\mu\mathcal{M} = ik\mu[\Phi-\Psi](k)\ , \tag{A1}$$

where k denotes the wave number and $\mu = \mathbf{n}\cdot\mathbf{k}/k$; $\mathbf{n}$ stands for the momentum direction of the relativistic particles. $\mathcal{M}$ is a gauge-invariant perturbation variable for the energy integrated one-particle distribution function,

$$\mathcal{M} = \frac{\pi}{\rho}\int p^3 dp \delta f \ .$$

Using the general definition of the energy momentum tensor,

$$T^{\mu\nu} = \int \frac{d^3p}{p^0} f(p) p^\mu p^\nu \ ,$$

we obtain

$$D_g = 2\int_{-1}^{1} \mathcal{M} d\mu \tag{A2}$$

$$V = \frac{3i}{2}\int_{-1}^{1} \mathcal{M}\mu d\mu \tag{A3}$$

$$\Pi = 3\int_{-1}^{1} (1-3\mu^2)\mathcal{M} d\mu \ . \tag{A4}$$

The gravitational perturbation equations on super-horizon scales yield

$$\Phi = \frac{1}{4}D_g + \frac{V}{x} + \frac{1}{6}x^2\Phi_s \tag{A5}$$

$$\Psi = -\Phi - 2\epsilon f_\pi - \frac{1}{x^2}\Pi \ , \tag{A6}$$

where $\Phi_s = \epsilon k^{-2}[f_\rho + (3/t)f_v]$. Furthermore, the conservation equation, $D_g' = -(4/3)V$, tells us that $D_g \propto xV$, so that we may neglect the D_g term in Eq. (A5). Inserting Eqs. (A5, A6) in Eq. (A1), we obtain

$$\partial_y \mathcal{M}(y,x) + i\mathcal{M} = i[\frac{2V}{x} + \frac{1}{3}x^2\Phi_s + 2\epsilon f_\pi + \frac{\Pi}{x^2}](k) \ , \tag{A7}$$

where $y = \mu x$.

For $x \ll 1$, and thus $y \ll 1$, we make the ansatz (see [21])

$$\mathcal{M} = x^\beta [c_1 y + c_2 y^2 + \mathcal{O}(y^3)] \ , \tag{A8}$$

where c_1, c_2 and β are constants. Inserting this ansatz in Eqs. (A2), (A3) and (A4), we get

$$D_g = \frac{4}{3}c_2 x^{\beta+2} \tag{A9}$$

$$V = ic_1 x^{\beta+1} \qquad = -(\beta+2)c_2 x^{\beta+1} \tag{A10}$$

$$\Pi = -\frac{8}{5}c_2 x^{\beta+2} \ , \tag{A11}$$

where the second equality in Eq. (A10) is obtained from the energy conservation equation (the zeroth moment of Eq. (A1)). The first moment of Eq. (A1) (momentum conservation) implies

$$[(\beta+2)(\beta+3) + \frac{8}{5}]c_2 x^\beta = \frac{1}{3}x^2\Phi_s + 2\epsilon f_\pi \ . \tag{A12}$$

If $\epsilon f_\pi \lesssim x^2\Phi_s$, Eq. (A12) leads to $\mathcal{O}(V/x) = \mathcal{O}(\Pi/x^2) = \mathcal{O}(x^2\Phi_s) = \mathcal{O}(x^2\Psi_s)$. Thus, $\mathcal{O}(\Phi) = \mathcal{O}(x^2\Phi_s)$ and $\mathcal{O}(\Psi) = \mathcal{O}(x^2\Psi_s)$ which means that we find compensation. In the other case, $f_\pi \gg x^2\Phi_s$, the right hand side of Eq. (A12) behaves like $\epsilon f_\pi \propto 1/x^2$, implying $\beta = -2$. Eq. (A12) then leads to

$$-\Pi/x^2 = \frac{8}{5}c_2 x^\beta \sim 2\epsilon f_\pi \qquad \text{and} \qquad V \sim 0 \ .$$

Inserting this in Eqs. (A5, A6) yields

$$\Psi = -\Phi = -\frac{1}{6}x^2\Phi_s \ , \tag{A13}$$

and thus $\mathcal{O}(\Phi) = \mathcal{O}(x^2\Phi_s)$ and $\mathcal{O}(\Psi) \leq \mathcal{O}(x^2\Psi_s)$, leading again to compensation.

We thus have shown that in this example, compensation is present even if the anisotropic stresses of the seeds are not suppressed.

References

[1] P.J. Steinhard, "Cosmology at the Crossroads", to appear in the *Proceedings of the Snowmass Workshop on Particle Astrophysics and Cosmology*, E. Kolb and R. Peccei, eds. (1995), astro-ph/9502024.

[2] T.W.B. Kibble, *Phys. Rep.* **67**, 183 (1980).

[3] J. Magueijo, A. Albrecht, P. Ferreira and D. Coulson, "The structure of Doppler peaks induced by active perturbations", astro-ph/9605047 (1996).

[4] H.R. Harrison, *Phys. Rev.* **D1**, 2726 (1970).

[5] Y.B. Zel'dovich, *Mon. Not. Roy. Ast. Soc.* **160**, 1 (1972).

[6] W. Hu and N. Sugyiama, *Astrophys. J.* **444**, 489 (1995); W. Hu and N. Sugyiama, *Phys. Rev.* **D51**, 2599 (1995).

[7] R. Durrer, A. Gangui and M. Sakellariadou, *Phys. Rev. Lett.* **76**, 579 (1996).

[8] R. Crittenden and N. Turok, *Phys. Rev. Lett.* **75**, 2642 (1995)
(In this work the amplitude of the first acoustic peak is substantially overestimated. In a recent preprint, astro-ph/9704165, this has been corrected and is now basically in agreement with our result in [7].)
A. Albrecht et al., *Phys. Rev. Lett.* **76**, 1413 (1996).

[9] N. Turok, *Phys. Rev. Lett.*, **63**, 2625 (1989).

[10] R. Durrer and Z.H. Zhou, *Phys. Rev.* **D53**, 5384 (1996).

[11] R. Durrer, *Phys. Rev.* **D42**, 2533 (1990).

[12] R. Durrer, *Fund. of Cosmic Physics* **15**, 209 (1994).

[13] W. Hu and N. Suguyama, "Small scale cosmological perturbations: an analytic approach", astro-ph/9510117 (1996).

[14] H. Kodama and M. Sasaki, *Prog. Theor. Phys. Suppl.* **78**, 1 (1984).

[15] J. Traschen, *Phys. Rep.* **29**, 1563 (1984).

[16] S. Veeraghavan and A. Stebbins, *Astrophys. J.* **365**, 37 (1990).

[17] W. Hu, D.N. Spergel and M. White, *Phys. Rev.* **D55**, 3288 (1997).

[18] M. Kunz and R. Durrer, *Phys. Rev.* **D55**, R4516 (1997).

[19] N. Turok, *Phys. Rev. Lett.* **77**, 4138 (1996).

[20] U.-L. Pen, D.N. Spergel and N. Turok, *Phys. Rev.* **D49**, 692 (1994).

[21] P.J.E. Peebles, *Astrophys. J.* **180**, 1 (1973).

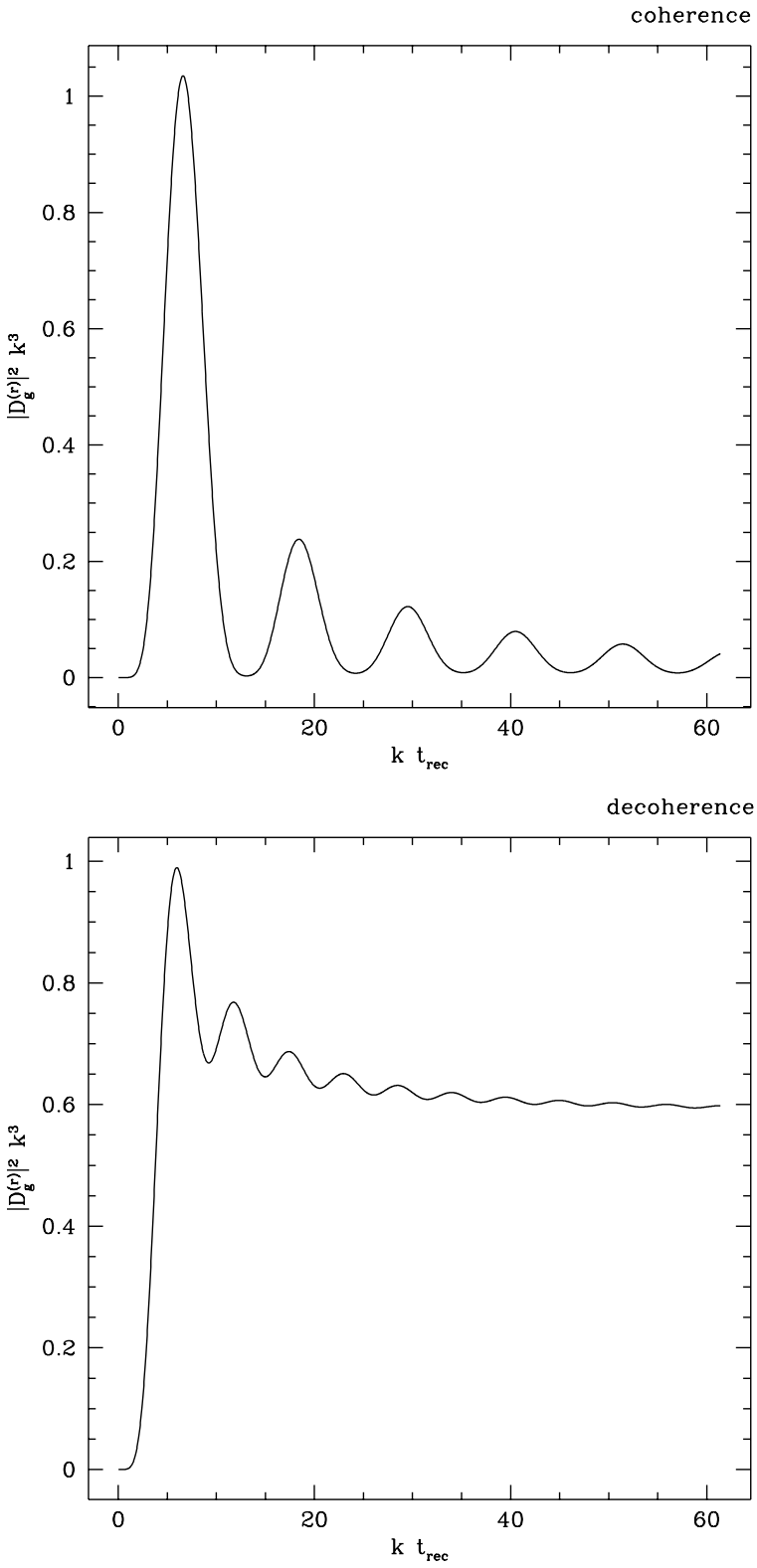

Figure 1: The acoustic fluctuations in the photon density spectrum are shown for the case of perfect coherence, (top) and complete decoherence (bottom).

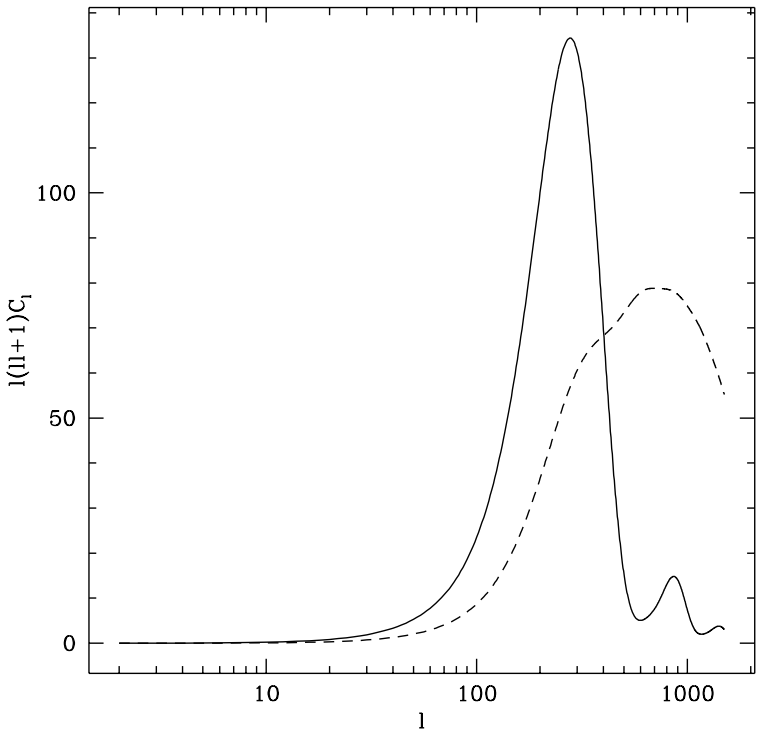

Figure 2: The resulting spectrum of CMB anisotropies from the photon density perturbations given in Fig. 1 for perfect coherence (solid line) and complete decoherence (dashed line).

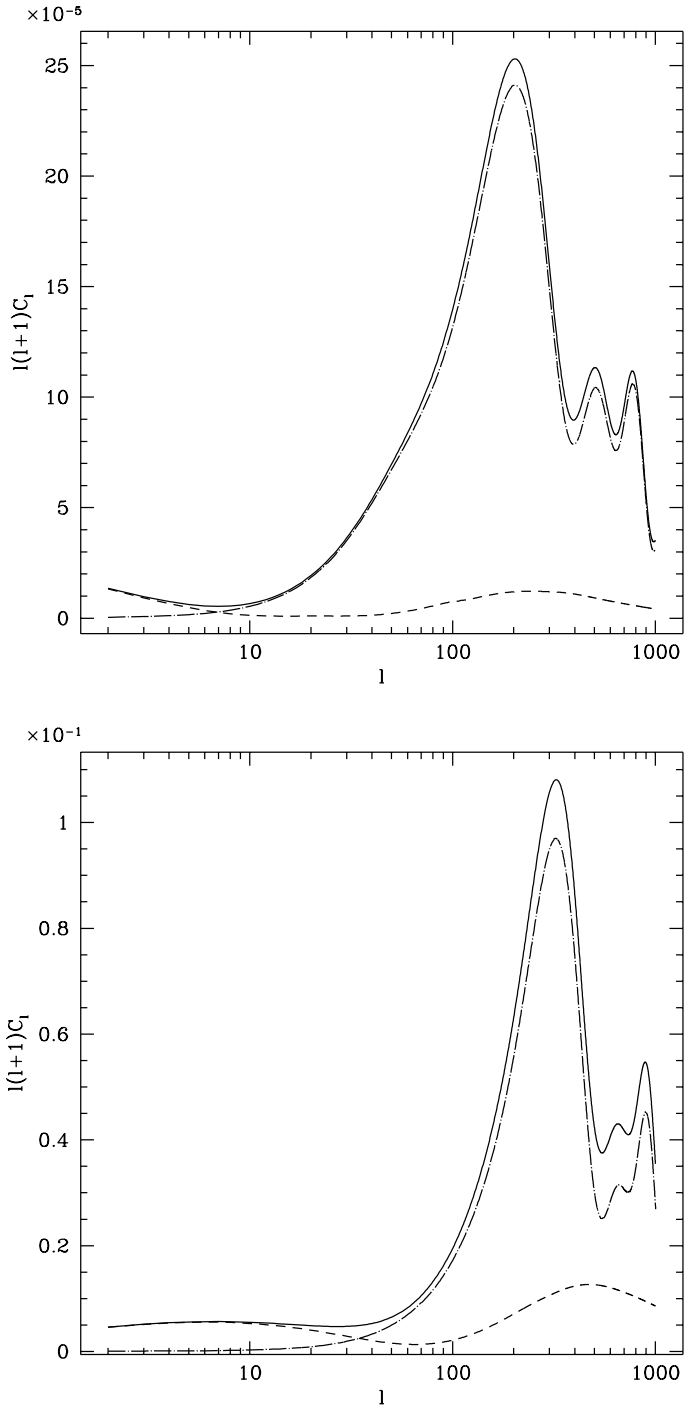

Figure 3: Here and in the subsequent figures, the CMB anisotropies are shown in units of $\epsilon^2 = (4\pi G\eta^2)^2$. The Sachs Wolfe contribution alone is indicated by a dashed line and the coherent sum of acoustic and Doppler terms are shown as dot-dashed curve. The solid line is the incoherent sum of these two contributions. Here the seed functions are determined by the choice $A_1 = 3$, $A_3 = -0.6$ and $A_4 = 0$. In the top frame the seed functions decay exponentially, while they decay like a power law in the bottom one.

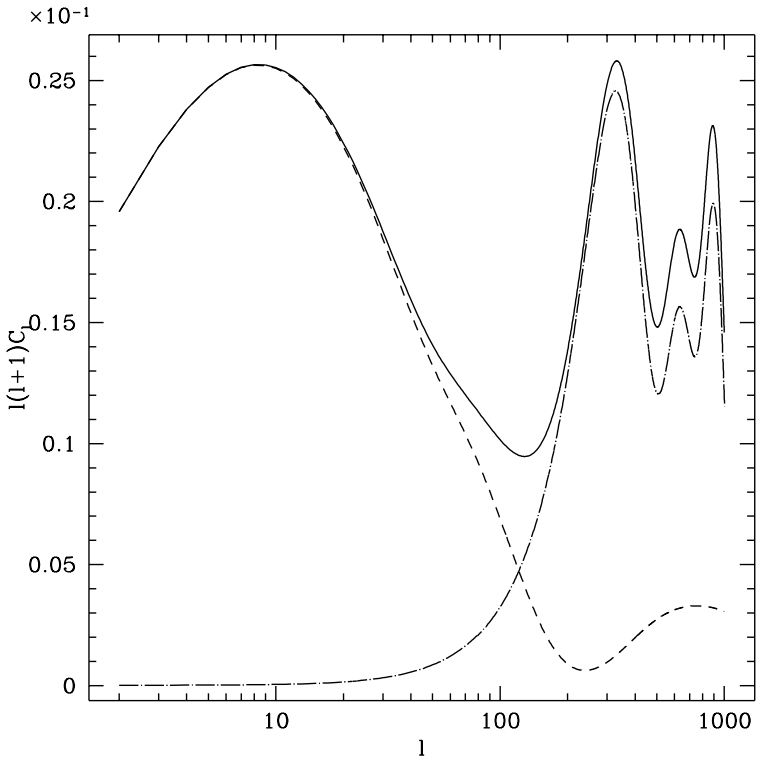

Figure 4: As Fig. 3b, but with $A_3 = -0.7$. In this regime ($A_4 = 0$, $A_3 \sim -(1/4$ to $1/3)A_1$) the resulting spectrum depends very sensitively on A_3. While $A_3 = -0.6$ leads to a perfectly reasonable spectrum with a somewhat high first acoustic peak, this spectrum is excluded by observations due to its "bump" in the Sachs Wolfe plateau and the absence of a distinctive acoustic peak.

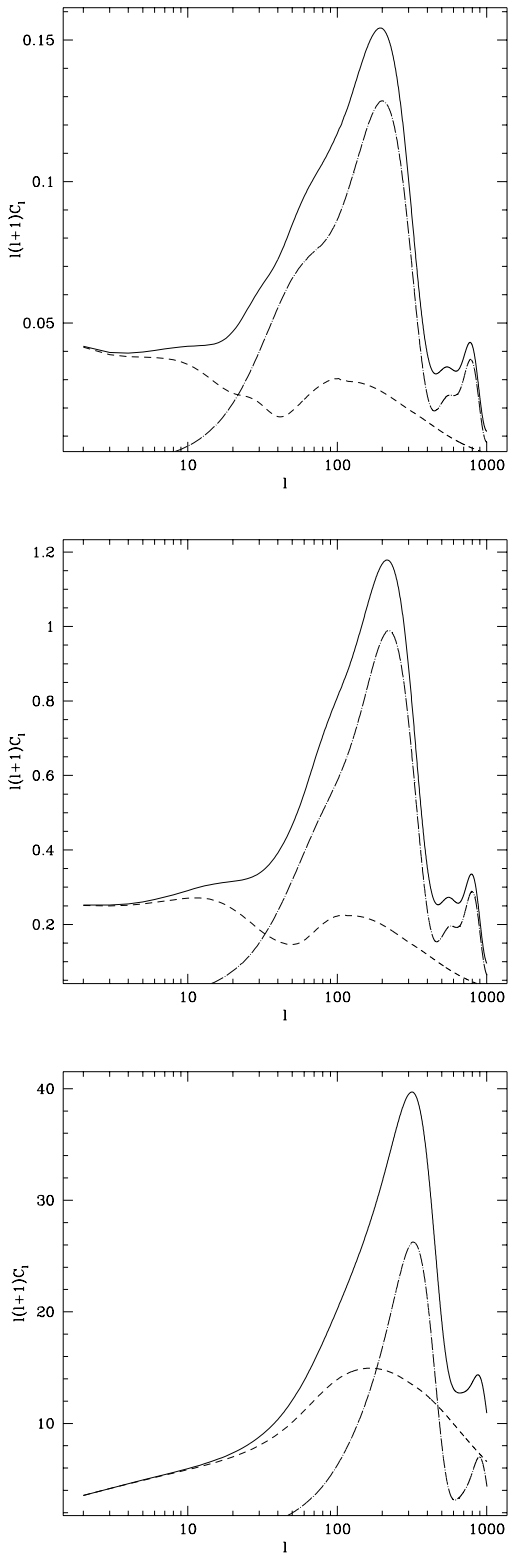

Figure 5: The CMB anisotropy spectrum for parameters $A_1 = 3$, $A_3 = 1$, $A_4 = 2$ and exponential decay, $F_i \propto \exp(-x^2)$ (top) and $F_i \propto \exp(-x^2/2)$ (middle). The corresponding spectrum for seed functions with power law decay is shown in the bottom frame. The position and relative amplitude of the first acoustic peak of the spectra (top) and (middle) is comparable with an inflationary spectrum. This simple example hints that it may be possible to "manufacture" inflationary spectra by choosing suitable seed functions.

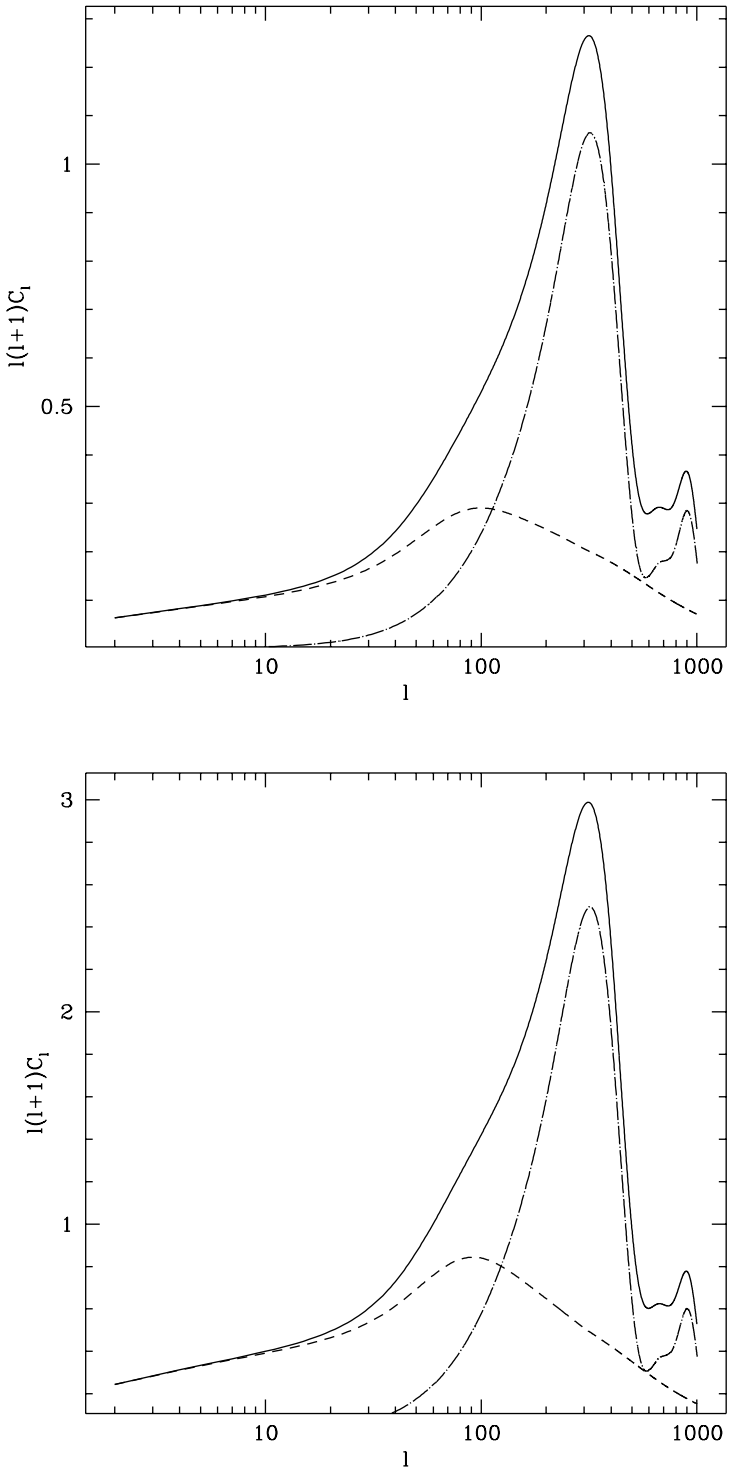

Figure 6: The anisotropy spectra for $A_1 = 3$, $A_4 = A_1/6(2\pi)^2$ and $A_3 = A_1/18$ (top) respectively $A_3 = -A_1/18$ (bottom) are shown. The seed functions are chosen to have power law decay. These are the values A_i which can be inferred from energy momentum conservation under the assumption of perfect coherence (see text). The sign of A_3 cannot be deduced, but we see that the results do not depend on it.

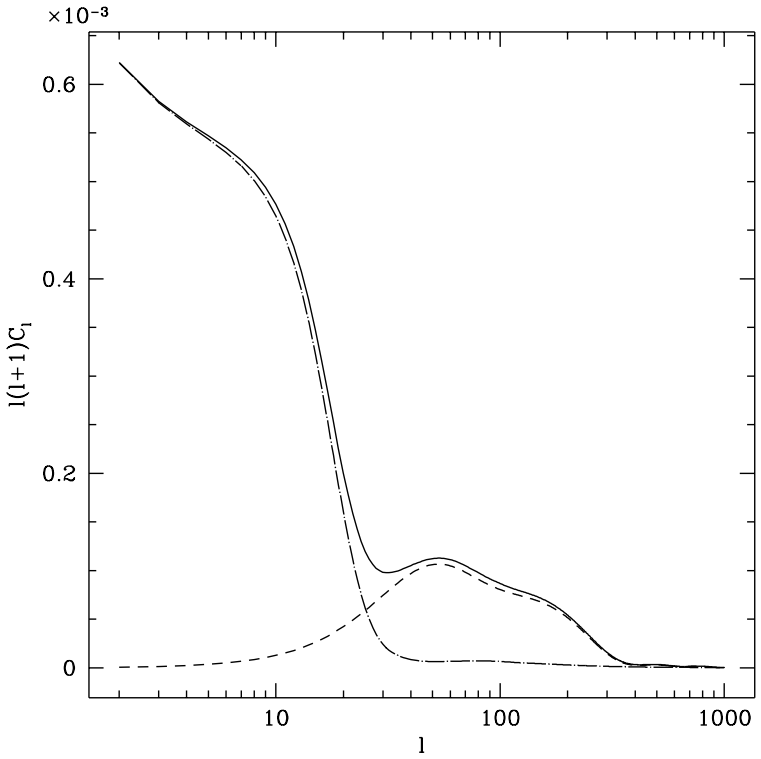

Figure 7: Even extremely strange spectra, like this one with a negative spectral index and without acoustic peaks can be obtained. For this result we have chosen exponentially decaying source functions, $F_i \propto \exp(-x^2)$ and $A_1 = 3$, $A_3 = -1$, $A_4 = 0$.

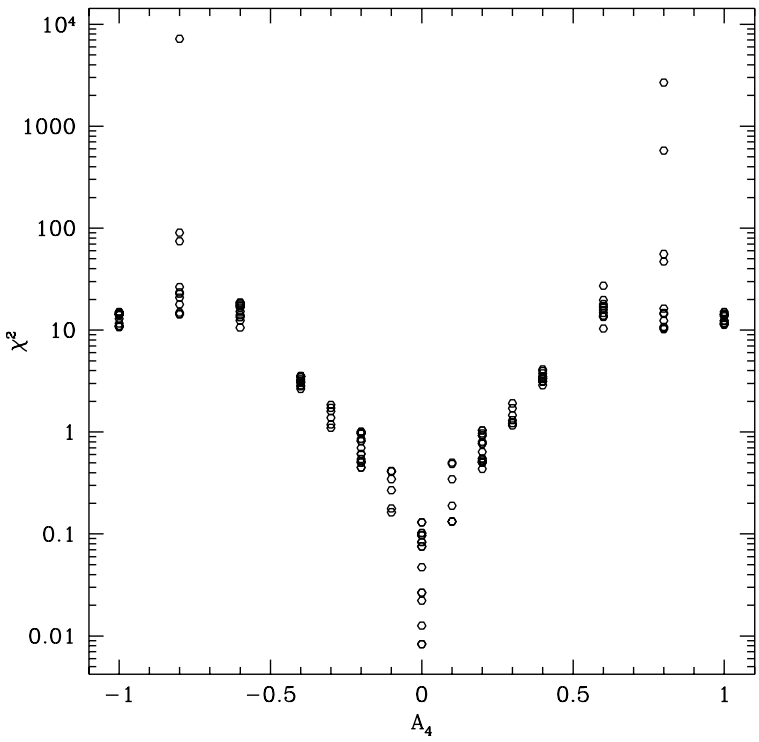

Figure 8: The CMB anisotropies on large scales, $\ell \leq 20$ from 122 models with scaling sources with structure function amplitudes (for details see text) in the regime $-1 \leq A_4/A_1 \leq 1$ and $-1 \leq A_3/A_1 \leq 1$ are fitted to simple power law spectra with spectral index $-0.5 \leq n \leq 2.5$. The χ^2 of the fit (allowing for 5% relative error) is shown as function of A_4.

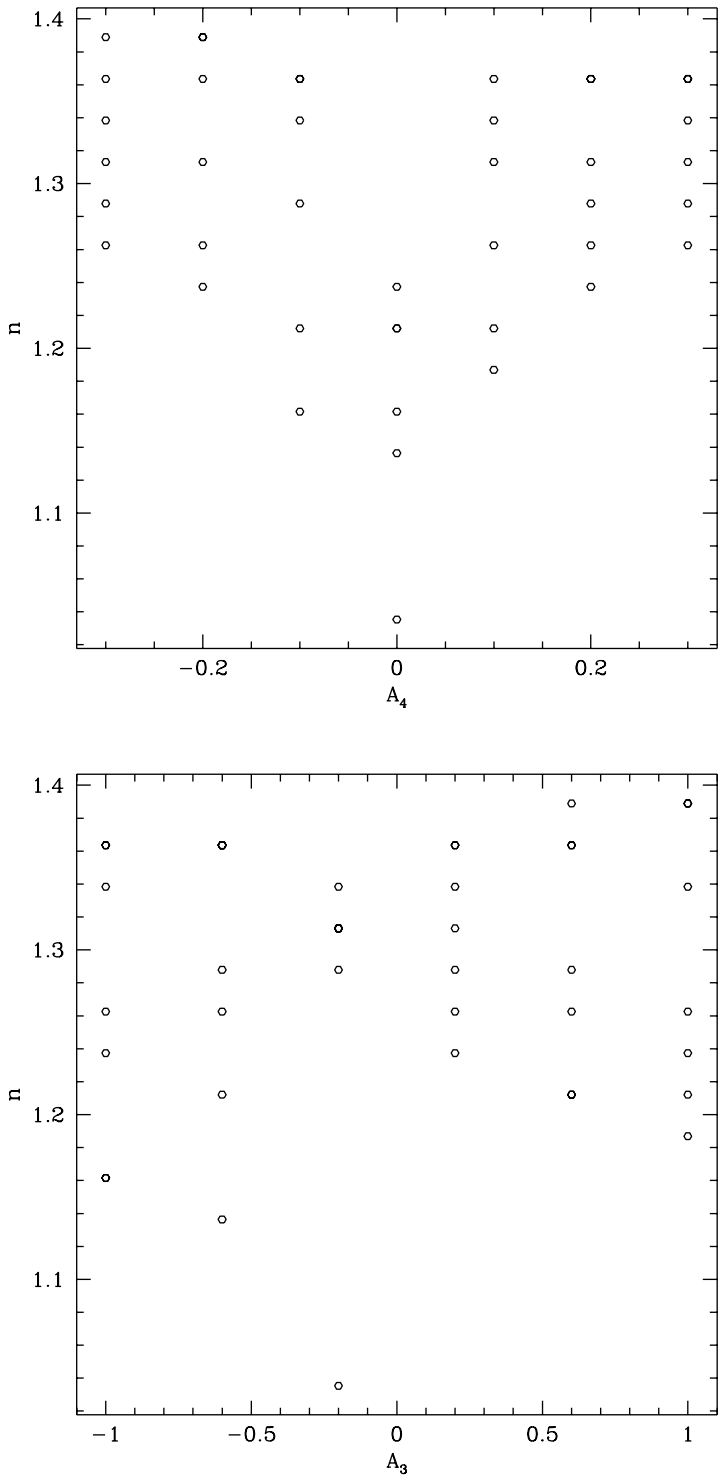

Figure 9: The spectral index for different models with $-0.3 \leq A_4/A_1 \leq 0.3$ and $-1 \leq A_3/A_1 \leq 1$ is shown as function of A_4 (top). The fact that there are less than six different circles visible for some values of A_4 is due to the discrete spacing of about 0.06 in n. The bottom frame shows the same results as a function of A_3.

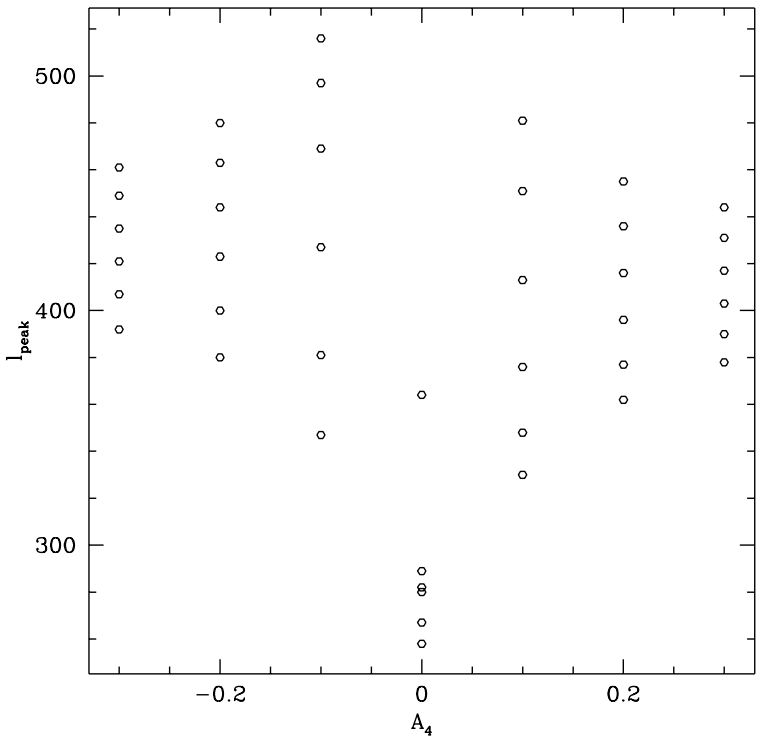

Figure 10: The position of the first acoustic peak is shown as function of A_4/A_1 for different values of A_3 in the range $-A_1 \leq A_3 \leq A_1$.

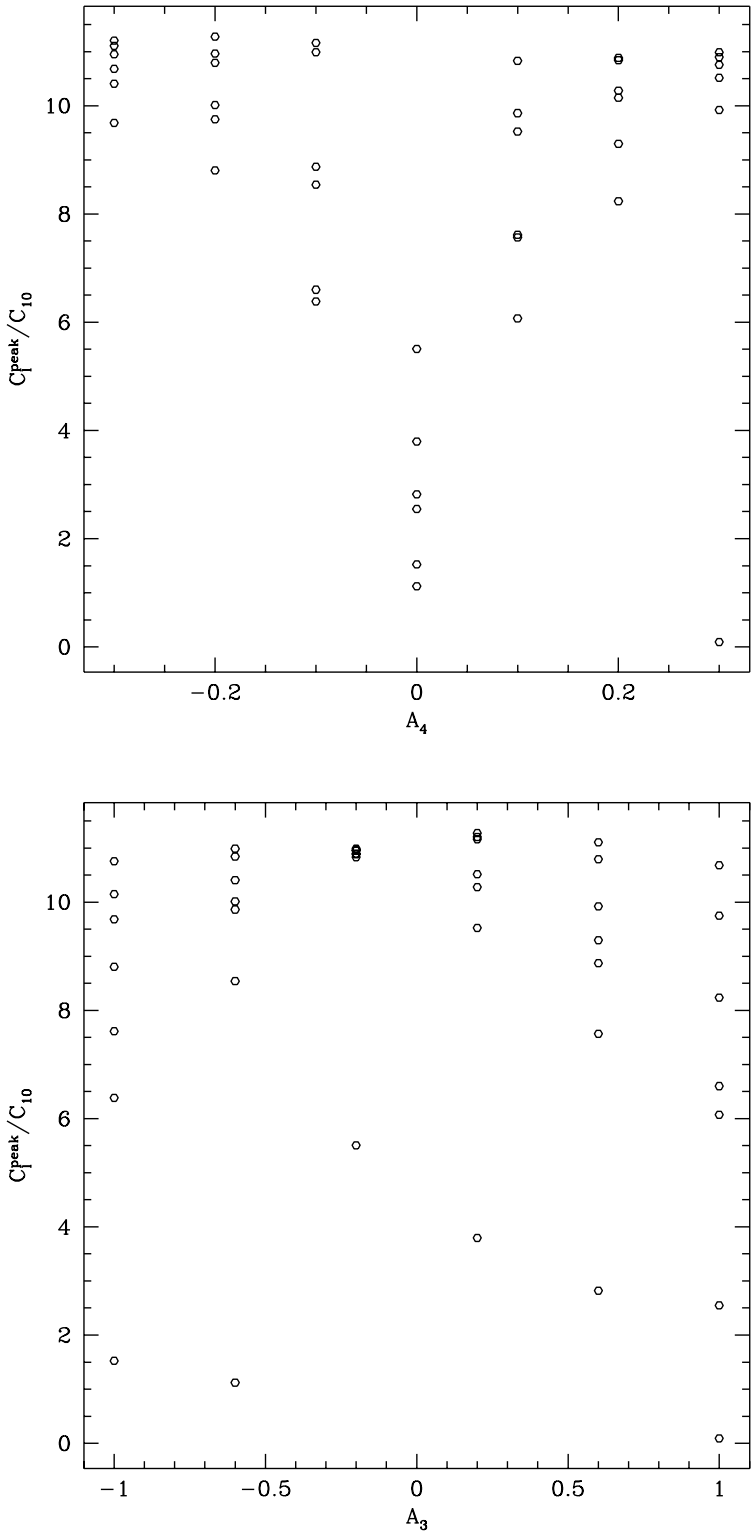

Figure 11: The amplitude of the first acoustic peak over the Sachs Wolfe plateau is shown as function of A_4/A_1 (top) for different values of A_3 in the range $-A_1 \leq A_3 \leq A_1$. The bottom frame shows the same results as a function of A_3.

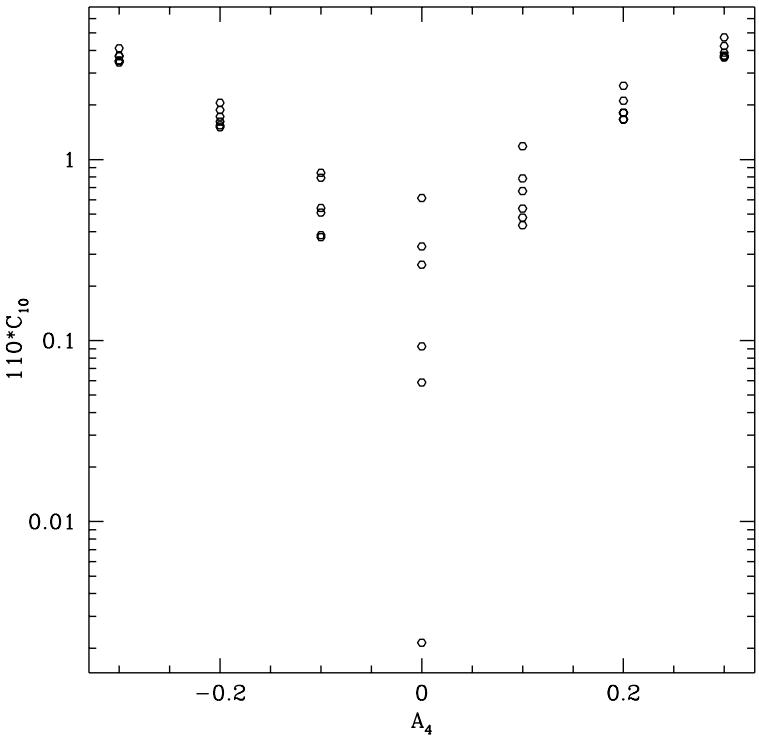

Figure 12: The amplitude $110C_{10}$ is given (in units of $\epsilon^2 A_1^2$) as a function of the amplitude of anisotropic stresses, A_4/A_1. It varies over about 3 orders of magnitudes and can become substantially smaller than 1, especially for very small values of A_4. The significance of this finding for the biasing problem is discussed in the text.